



ARTICLE

Esterification reaction kinetics of acetic acid and n-pentanol catalyzed by sulfated zirconia

Fabiane Hamerski | Giovana Gonçalves Dusi | Julia Trancoso Fernandes dos Santos | Vítor Renan da Silva | Fernando Augusto Pedersen Voll | Marcos Lúcio Corazza

Department of Chemical Engineering,
Federal University of Paraná (UFPR),
Curitiba, PR, Brazil

Correspondence

Vítor Renan da Silva, Department of Chemical Engineering, Federal University of Paraná, Francisco H. Santos Av. 100, Curitiba, Paraná, Brazil.
Email: vrenan@ufpr.br

Funding information

CNPq, Grant/Award Numbers: 1688/2018, 305393/2016-2, 435873/2018-0; CAPES; Conselho Nacional de Desenvolvimento Científico e Tecnológico, Grant/Award Numbers: 1688/2018, 305393/2016-2, 435873/2018-0

Abstract

This study reports experimental data and kinetic modeling of acetic acid esterification with *n*-pentanol using sulfated zirconia as a catalyst. Reactions were carried out in an isothermal well-mixed batch reactor at different temperatures (50–80°C), *n*-pentanol to acid molar ratios (1:1–3:1), and catalyst loadings (5–10 wt% in relation to the total amount of acetic acid). The reaction mechanism regarding the heterogeneous catalysis was evaluated considering pseudo-homogeneous, Eley–Rideal, and Langmuir–Hinshelwood model approaches. The reaction mixture was considered a nonideal solution and the UNIQUAC thermodynamic model was used to take into account the nonidealities in the liquid phase. The results obtained indicated that increases in the temperature and catalyst loading increased the product formation, while changes in the *n*-pentanol to acetic acid molar ratio showed no significant effect. The estimated enthalpy of the reaction was $-8.49 \text{ kJ mol}^{-1}$, suggesting a slightly exothermic reaction. The Eley–Rideal model, with acetic acid adsorbed on the catalyst as the limiting step, was found to be the most significant reaction mechanism.

KEYWORDS

Eley–Rideal, esterification, Langmuir–Hinshelwood, pentyl ethanoate, sulfated zirconia

1 | INTRODUCTION

Organic esters are important fine chemicals widely used in a variety of areas including food, pharmaceuticals, cosmetics, biofuels, and chemical industries. These compounds are used as additives, plasticizers, solvents, or intermediates and can be obtained through the transesterification or esterification of either carboxylic acids or fatty acids with an alcohol.^{1–4} In the food industry in particular, the organic esters derived from fatty acids can be used as emulsifiers,⁵ and the acetate and ethyl esters act as primary odorants in the perceptual response of fruity aroma in food products, such as beverage, wine, and juices.⁶ Similarly, amyl acetate (pentyl ethanoate) is an important component of different fruit flavors (eg, pear, apple, and banana).^{7,8} Chemical synthesis is an alternative way to produce these organic esters and the most common route is the

direct esterification of carboxylic acids with alcohols in the presence of acid catalysts.⁹

Esterification is conventionally carried out using homogeneous catalysts with strong mineral acids, such as sulfuric acid and *p*-toluenesulfonic acid. However, this chemical route is associated with several drawbacks in industrial applications:^{9,10} (a) acid catalyst recovery is economically expensive; (b) high operational and installations costs due to the increases of corrosion rates; and (c) high costs of wastes removal, treatment, and disposal of the homogeneous catalyst; Thus, the use of a solid acid catalyst in heterogeneous catalysis represents an alternative to the homogeneous reaction process with advantages including: (a) the catalyst is solid, nontoxic, and reusable; (b) corrosion in the reactor system is reduced; and (c) the catalyst can be easily separated from the reaction mixture by a physical process, such as filtration.¹¹

Sulfated metal oxides with both Brønsted and Lewis acid sites have been widely proposed and used as solid acid catalysts and/or supports in organic synthesis, including esterification reactions.¹² Sulfated zirconia ($\text{SO}_4\text{-ZrO}_2$) is a solid catalyst of particular interest because it has high thermal stability, low cost, and presents a high amount of acid sites with a Hammett acidity function of around -16.1 .¹³ These properties have led to its application as a catalyst in isomerization and alkylation processes^{14–16} and Fischer's esterification reactions.^{17–20}

In order to describe the kinetic behavior of heterogeneous catalytic esterification reactions, several kinetic models have been proposed in the literature. In some reaction systems, such as a heterogeneous esterification of free fatty acids to biodiesel and emulsifiers,^{17,21,22} the kinetic behavior of the reactions can approach by the pseudo-homogeneous (PH) model. On the other hand, several authors studying esterification reactions with heterogeneous catalysts have proposed mechanisms that involve surface phenomena for the interaction between the reactant and active sites on the catalyst surface, which have been successfully described by Langmuir–Hinshelwood (LH) and Eley–Rideal (ER) models.^{2,23–26} The LH model is applicable for correlating the kinetics data whenever the reaction occurs between the intermediate species, formed by chemical adsorption of the reactants on the active sites of the catalyst surface, while the ER model is normally applied when the reaction occurs between an adsorbed species and a species in the bulk liquid phase (non-adsorbed species).²⁷

Some studies have shown that both LH and ER models can describe the mechanism involved in the kinetics of solid acid zirconia-catalyzed esterification reactions.^{11,20,28,29} However, to the best of our knowledge, there are no reports in the literature considering a detailed study and kinetic modeling of pentyl ethanoate synthesis by the Fischer esterification reaction with sulfated zirconia as the heterogeneous catalyst. Thus, this work aims to bring a new set of experimental data and the kinetic modeling investigation of acetic acid esterification with n-pentanol using a sulfated zirconia-catalyst system.

2 | EXPERIMENTAL

2.1 | Synthesis of sulfated zirconia

The sulfated zirconia was prepared based on the procedure described by Corma et al.³⁰ Briefly, under magnetic stirring, 50 mL of an aqueous solution (0.4 mol L^{-1}) of zirconium (IV) oxychloride octahydrate (Vetec; 99.5%, Duque de Caxias, Rio de Janeiro, Brazil) was added drop by drop to a beaker containing distilled water (15 mL) at pH 10. The pH was maintained constant during the precipitation by adding an ammonia solution (Vetec; 26%, Duque de Caxias, Rio de Janeiro,

Brazil) and it was monitored using a digital pH-meter. The total volume of ammonia solution used during the precipitation process was approximately 12 mL. The suspension obtained was maintained for 2 h under vigorous stirring, at room temperature. The precipitate was filtered, washed with distilled water until free of chlorine (verified by testing with an aqueous solution of AgNO_3) and dried at 100°C for 16 h. The solid phase comprised of zirconium hydroxides were crushed to a fine powder and impregnated with a 0.5 mol L^{-1} H_2SO_4 solution (5 mL of solution per 1 g of solids) for 2 h. The solids were then filtered, dried at 100°C for 16 h, and calcined at 550°C for 3 h.

2.2 | Characterization of sulfated zirconia

X-ray diffraction (XRD) data were collected on a Panalytical X-ray powder diffractometer (Cambridge, United Kingdom) using Cu K_α radiation ($\lambda = 1.5406 \text{ \AA}$, 40 kV, and 30 mA), at 2θ , in the range of $20\text{--}80^\circ$ with a step size of 0.02. Raman mapping was carried out using a confocal Raman microscope (Witec-alpha 300R, Ulm, Germany), with objective magnification (10 \times), a power of 32.9 mW and a 532 nm frequency-doubled Nd:YAG laser with a resolution of 0.02 cm^{-1} .

Fourier transform infrared (FTIR) spectra of the sulfated zirconia were obtained at room temperature in the wavenumber range of $4000\text{--}400 \text{ cm}^{-1}$, with a resolution of 4 cm^{-1} and 32 scans, on a BIO-RAD, Excalibur Series (FTS 3500GX) spectrophotometer (New York, USA). Pellets of the sample were prepared for the analysis by mixing the fine catalyst powder with KBr (Vetec; spectroscopic grade) in a weight ratio of 1:10.

Thermogravimetric (TG) and differential scanning calorimetric (DSC) analyses were carried out with a Netzsch analyzer (STA 449 F3 Jupiter, Selb, Germany), using approximately 5 mg of sample, alumina crucibles, nitrogen atmosphere, and a heating rate of $10^\circ\text{C min}^{-1}$, in the temperature range of $20\text{--}1000^\circ\text{C}$.

The specific surface area and pore size distribution were determined using the Brunauer–Emmett–Teller (BET) method,³¹ with the N_2 adsorption and desorption isotherms obtained at -163°C on a NOVA-1200 Quantachrome instrument (Boynton Beach, Florida, USA).

The particle size distribution and average diameter of sulfated zirconia particles were obtained using an automated particle size analyzer (CILAS; model 1064, Orleans, France). Firstly, to have proper sample dispersion, the sulfated zirconia ($\sim 10 \text{ mg}$) was added to distilled water in the liquid dispersion unit of the equipment. The dispersed sample was pumped into a glass measurement cell, which is placed in front of the laser and it was kept circulating until the end of the measurements. The detected diffraction pattern was analyzed by software *The Particle Expert* and the particle size distribution and average diameter of the sulfated zirconia powder was obtained.

The surface morphology and composition of the sulfated zirconia were determined, respectively, by scanning electron microscopy (SEM) and energy dispersion spectroscopy (EDS) using a Tescan VEGA-3 LMU microscope (Kohoutovice, Czech Republic). Results of elemental composition by EDS are average values of measurements obtained on three different location of the catalyst sample.

2.3 | Reaction procedure

Esterification was used for the synthesis of pentyl ethanoate (n-amyl-acetate) performed by reacting acetic acid and *n*-pentanol, as shown in the following equation:



Kinetics study of the pentyl ethanoate esterification catalyzed by sulfated zirconia was performed in a 40 mL jacketed glass reaction vessel (diameter of 3.5 cm and height of 6.0 cm), equipped with a magnetic stirrer (magnetic bar of 2 cm length), and coupled to a thermostatic bath with external circulation (Vivo RT4). All reactions were performed in a batch mode. The temperature ranged from 50 to 80°C. The catalyst concentration in the reaction mixture was varied from 5.0 to 10 wt%, related to the total amount of acetic acid. The initial *n*-pentanol to acetic acid molar ratio was varied from 1:1 to 3:1. The stirring speed was fixed at 500 rpm for all experiments. A measured amount (weighted) of acetic acid and catalyst were added to the reactor and the temperature of the reactor was set to the reaction temperature setpoint. An amount of *n*-pentanol (according to the pre-established initial reactant molar ratio) was preheated and added to the reactor and the reaction was started. Samples (around 300 μL) were collected during the reaction time and submitted to titration with NaOH solution (0.1 mol L⁻¹, standardized with potassium hydrogen phthalate) for the calculation of acetic acid consumption. The sum of the samples withdrawn from the reactor for titration was less than 10% of the total volume of the reaction to avoid significant variations in the reactant volume, which could interfere with the reaction.⁴ The amounts of *n*-pentanol, pentyl ethanoate and water were obtained from a stoichiometric balance for the esterification reaction.

The software *Statistica 7.0*TM was used for the statistical analysis (ANOVA effects) to evaluate the effects of temperature and the *n*-pentanol to acetic acid molar ratio. The effect of the solid catalyst concentration on the esterification conversion was evaluated by kinetics studies carried out at 70°C with a *n*-pentanol to acetic acid molar ratio of 3:1. The conversion (X_{AC}) and the observed reaction rate for acetic acid (r_{AC}) were calculated as follows:

$$X_{\text{AC}} = \frac{\text{moles of acetic acid consumed}}{\text{initial moles of acetic acid}} \quad (2)$$

$$r_{\text{AC}} = \frac{\text{moles of AC consumed in reaction time (mol)}}{\text{catalyst loading} \times \text{reaction time (g)} \times (\text{min})} \quad (3)$$

Additional experiments of homogeneous reaction were performed using 1.0 wt% of H₂SO₄ (Vetec; 98% of purity) in relation to the total amount of acetic acid. The homogeneous reactions were carried out at temperatures of 50-80°C, with a fixed *n*-pentanol to acetic acid molar ratio of 3:1 and stirring speed of 500 rpm, using the same reactor setup used in the heterogeneous reactions.

Equilibrium data were evaluated using the software *Aspen Plus v.8.4* (Aspen Technology, Inc, Bedford, Massachusetts, USA). The activity coefficients and molar fractions of all species at equilibrium were calculated by the Rigorous Reactor Model based on Gibbs free energy minimization, where the UNIQUAC thermodynamic model was used to calculate the non-ideality corrections of all compounds in the phase liquid. The reaction equilibrium constant (K_{EQ}) was evaluated by Equation 4:³²

$$K_{\text{EQ}} = \frac{a_{\text{AC,EQ}} \times a_{\text{P,EQ}}}{a_{\text{E,EQ}} \times a_{\text{W,EQ}}} = \left(\frac{x_{\text{AC,EQ}} \times x_{\text{P,EQ}}}{x_{\text{E,EQ}} \times x_{\text{W,EQ}}} \right) \times \left(\frac{\gamma_{\text{AC,EQ}} \times \gamma_{\text{P,EQ}}}{\gamma_{\text{E,EQ}} \times \gamma_{\text{W,EQ}}} \right) \quad (4)$$

where $a_{i,\text{EQ}}$ is the activity of species *i* (P, *n*-pentanol; AC, acetic acid; E, pentyl ethanoate; W, water) at equilibrium, $x_{i,\text{EQ}}$ is the molar fraction of species *i* at equilibrium, and γ_i is the activity coefficient of species *i* at equilibrium. The enthalpy of the reaction (ΔH°) was estimated by the integrated form of the Van't Hoff equation, assuming it as constant in the temperature range evaluated (Equation 5).

$$\frac{dn(K_{\text{EQ}})}{dT} = \frac{\Delta H^\circ}{R \times T^2} \quad (5)$$

2.4 | Kinetic modeling

In this study, the kinetic modeling of the esterification of acetic acid with *n*-pentanol catalyzed by sulfated zirconia was carried out using different approaches. The reaction mechanisms evaluated were PH, LH, and ER. Depending on the assumptions regarding the reaction mechanism and the rate-controlling step, different models can be development: (a) the PH model assumes that the adsorption and desorption steps can be neglected; (b) the LH model assumes that both reactants are adsorbed onto the active sites of the catalyst; and (c) the ER model assumes that one of the adsorbed reactants reacts with another in the bulk phase. Table 1 summarizes all reaction rate equations derived from the mechanisms evaluated. In the first column, the nomenclature adopted to identify each equation is indicated, while the reaction mechanism (PH, LH, or ER) and the rate-controlling step (adsorption, surface reaction, or desorption) are presented in the second and third columns, respectively.

In Table 1, M_{cat} is the amount of catalyst in g, a_i is the activity of species *i* ($a_i = \gamma_i x_i$), γ_i is the activity coefficient

TABLE 1 Reaction rate equations for different reaction mechanisms

Model name	Mechanism	Rate controlling step	Rate equation
PH	Pseudo-homogeneous	Surface reaction	$r_i = M_{\text{cat}} \times k_f \times \left[a_{\text{AC}} \times a_p - \frac{a_E \times a_W}{K_{\text{EQ}}} \right]$
LH_AD_AC		Adsorption of the acetic acid	$r_i = \frac{M_{\text{cat}} \times k_{\text{ADS,AC}} \times \left[a_{\text{AC}} - \frac{a_E \times a_W}{a_p \times K_{\text{EQ}}} \right]}{1 + \frac{K_{\text{AC}}}{K_{\text{EQ}}} \times \frac{a_E \times a_W}{a_p} + K_P \times a_p + K_E \times a_E + K_W \times a_W}$
LH_AD_P	Langmuir–Hinshelwood Adsorbed acetic acid reacts with adsorbed <i>n</i> -pentanol	Adsorption of the <i>n</i> -pentanol	$r_i = \frac{M_{\text{cat}} \times k_{\text{ADS,P}} \times \left[a_p - \frac{a_E \times a_W}{a_{\text{AC}} \times K_{\text{EQ}}} \right]}{1 + K_{\text{AC}} \times a_{\text{AC}} + \frac{K_P}{K_{\text{EQ}}} \times \frac{a_E \times a_W}{a_{\text{AC}}} + K_E \times a_E + K_W \times a_W}$
LH_SR		Surface reaction	$r_i = \frac{M_{\text{cat}} \times k_f \times K_{\text{AC}} \times K_P \times \left[a_{\text{AC}} \times a_p - \frac{a_E \times a_W}{K_{\text{EQ}}} \right]}{[1 + K_{\text{AC}} \times a_{\text{AC}} + K_P \times a_p + K_E \times a_E + K_W \times a_W]^2}$
LH_DES_E		Desorption of pentyl ethanoate	$r_i = \frac{M_{\text{cat}} \times k_{\text{DES,E}} \times K_{\text{EQ}} \times \left[\frac{a_{\text{AC}} \times a_p}{a_W} - \frac{a_E}{K_{\text{EQ}}} \right]}{1 + K_{\text{AC}} \times a_{\text{AC}} + K_P \times a_p + K_P \times K_{\text{EQ}} \times \frac{a_{\text{AC}} \times a_p}{a_W} + K_W \times a_W}$
LH_DES_W		Desorption of water	$r_i = \frac{M_{\text{cat}} \times k_{\text{DES,W}} \times K_{\text{EQ}} \times \left[\frac{a_{\text{AC}} \times a_p}{a_E} - \frac{a_W}{K_{\text{EQ}}} \right]}{1 + K_{\text{AC}} \times a_{\text{AC}} + K_P \times a_p + K_E \times a_E + K_W \times K_{\text{EQ}} \times \frac{a_{\text{AC}} \times a_p}{a_E}}$
ER_AC_ADS	Eley–Rideal: Adsorbed acetic acid reacts with <i>n</i> -pentanol in the liquid phase	Adsorption of acetic acid	$r_i = \frac{M_{\text{cat}} \times k_{\text{ADS,AC}} \times \left[a_{\text{AC}} - \frac{a_E \times a_W}{a_p \times K_{\text{EQ}}} \right]}{1 + \frac{K_{\text{AC}}}{K_{\text{EQ}}} \times \frac{a_E \times a_W}{a_p} + K_W \times a_W}$
ER_AC_RS		Surface reaction	$r_i = \frac{M_{\text{cat}} \times k_f \times K_{\text{AC}} \times \left[a_{\text{AC}} \times a_p - \frac{a_E \times a_W}{K_{\text{EQ}}} \right]}{1 + K_{\text{AC}} \times a_{\text{AC}} + K_W \times a_W}$
ER_AC_DES_E		Desorption of pentyl ethanoate	$r_i = \frac{M_{\text{cat}} \times k_{\text{DES,E}} \times K_{\text{EQ}} \times \left[\frac{a_{\text{AC}} \times a_p}{a_W} - \frac{a_E}{K_{\text{EQ}}} \right]}{1 + K_{\text{AC}} \cdot a_{\text{AC}} + K_E \cdot K_{\text{EQ}} \cdot \frac{a_{\text{AC}} \cdot a_p}{a_W}}$
ER_AC_DES_W		Desorption of water	$r_i = \frac{M_{\text{cat}} \times k_{\text{DES,W}} \times K_{\text{EQ}} \times \left[\frac{a_{\text{AC}} \times a_p}{a_E} - \frac{a_W}{K_{\text{EQ}}} \right]}{1 + K_{\text{AC}} \times a_{\text{AC}} + K_W \times K_{\text{EQ}} \times \frac{a_{\text{AC}} \times a_p}{a_E}}$
ER_P_ADS	Eley–Rideal: Adsorbed <i>n</i> -pentanol reacts with acetic acid in the liquid phase	Adsorption of <i>n</i> -pentanol	$r_i = \frac{M_{\text{cat}} \times k_{\text{ADS,P}} \times \left[a_p - \frac{a_E \times a_W}{a_{\text{AC}} \times K_{\text{EQ}}} \right]}{1 + \frac{K_P}{K_{\text{EQ}}} \times \frac{a_E \times a_W}{a_{\text{AC}}} + K_W \times a_W}$
ER_P_RS		Surface reaction	$r_i = \frac{M_{\text{cat}} \times k_f \times K_P \times \left[a_{\text{AC}} \times a_p - \frac{a_E \times a_W}{K_{\text{EQ}}} \right]}{1 + K_{\text{AC}} \times a_{\text{AC}} + K_P \times a_p}$
ER_P_DES_E		Desorption of pentyl ethanoate	$r_i = \frac{M_{\text{cat}} \times k_{\text{DES,E}} \times K_{\text{EQ}} \times \left[\frac{a_{\text{AC}} \times a_p}{a_W} - \frac{a_E}{K_{\text{EQ}}} \right]}{1 + K_P \times a_p + K_E \times K_{\text{EQ}} \times \frac{a_{\text{AC}} \times a_p}{a_W}}$
ER_P_DES_W		Desorption of water	$r_i = \frac{M_{\text{cat}} \times k_{\text{DES,W}} \times K_{\text{EQ}} \times \left[\frac{a_{\text{AC}} \times a_p}{a_E} - \frac{a_W}{K_{\text{EQ}}} \right]}{1 + K_P \times a_p + K_W \times K_{\text{EQ}} \times \frac{a_{\text{AC}} \times a_p}{a_E}}$

M_{cat} is the mass of the catalyst in g. a_i is the activity of species i (P, *n*-pentanol; AC, acetic acid; E, pentyl ethanoate; W, water). k_f is the forward reaction rate constant ($\text{mol g}^{-1} \text{min}^{-1}$). K_{EQ} is the surface reaction equilibrium constant. K_i is the adsorption equilibrium constant for species i .

of species i in the liquid phase, k_f is the forward reaction rate constant ($\text{mol g}^{-1} \text{min}^{-1}$), K_{EQ} is the surface reaction equilibrium constant, and K_i is the adsorption equilibrium constant for species i . In order to represent the temperature (T) sensitivity on the reaction system, the forward reaction rate constant was expressed by an Arrhenius-like expression (Equation 6):

$$k_f = k_0 \times \exp\left(-\frac{E_A}{R \times T}\right) \quad (6)$$

where k_f is the effective kinetic constant, k_0 is the pre-exponential factor, E_A is the activation energy parameter, and R is the gas constant. The model parameters (k_0 , E_A , and K_i) were fitted to the experimental data obtained within the temperature range of 50–80°C by minimizing the least square objective function (RSS), as presented in Equation 7:

$$\text{RSS} = \sum_j^{N_{\text{obs}}} \left(X_j^{\text{exp}} - X_j^{\text{calc}}\right)^2 \quad (7)$$

where N_{obs} is the number of experimental observations (experimental data points) and X_j^{exp} and X_j^{calc} are the experimental and calculated values of acid acetic conversion, respectively. The fourth order Runge–Kutta method was used to solve the differential equations and the “GRG non-linear” optimization subroutine was used to minimize the objective function.

The mean relative error (%) (MRE) and root mean square deviation (RMSD) were calculated for each model according to Equations 8 and 9, respectively.

$$\text{MRE} (\%) = \frac{\sum_j^{N_{\text{obs}}} \left| \frac{X_j^{\text{exp}} - X_j^{\text{calc}}}{X_j^{\text{exp}}} \right|}{N_{\text{obs}}} \times 100 \quad (8)$$

$$\text{RMSD} (\%) = 100 \times \sqrt{\frac{\sum_j^{N_{\text{obs}}} \left(X_j^{\text{exp}} - X_j^{\text{calc}}\right)^2}{N_{\text{obs}}}} \quad (9)$$

In order to evaluate which model of those tested best represents the reaction mechanism of the esterification reaction under study, Fisher’s F -test (F) and the Akaike information criterion (AIC) were applied, according to Equations 10 and 11, respectively.³³

$$F = \frac{\frac{\sum_j^{N_{\text{obs}}} \left(X_j^{\text{calc}}\right)^2}{K}}{\frac{\text{SQR}}{(N_{\text{obs}} - K)}} \times 100 \quad (10)$$

$$\text{AIC} = N \times \ln \left[\frac{\text{SQR}}{N_{\text{obs}}} \right] + 2 \times K \times \left[1 + \frac{K + 1}{N_{\text{obs}} + K - 1} \right] \quad (11)$$

where K is the number of fitted parameters in the model evaluated.

As mentioned above, the UNIQUAC model was used to calculate the activity coefficients for all components in the liquid phase. The binary interaction parameters were used as presented by Lee and Liang,³⁴ and they are reported in the Supplementary Material.

2.5 | Mass transfer phenomena

The effects of external and internal mass transfer limitations were also evaluated. The external mass transfer is directly related to the hydrodynamics of the reactant mixture during the reaction in the batch reactor and it is determined by the stirring speed. In order to assess this parameter, kinetic runs were carried out varying the stirring speed (50, 250, 500, and 700 rpm), at a fixed n-pentanol to acetic acid molar ratio of 3:1, 70°C, and catalyst concentration of 10 wt%. Also, the Mears criterion (C_M) was examined for the kinetic runs at different temperatures, calculated according to Equation 12:[27]

$$C_M = \frac{r_{\text{AC, OBS}} \times \rho_L \times R_p \times n}{k_C \times C_{\text{AC}}} \quad (12)$$

where $r_{\text{AC, OBS}}$ is the experimental value of the reaction rate at a given time, n is the reaction order, ρ_L is the density of the liquid reaction mixture, R_p is the catalyst particle radius, C_{AC} is the acetic acid concentration in the liquid reaction mixture, and k_C is the external mass transfer parameter. For a reaction system with C_M lower than 0.15, the external mass diffusion resistance can be neglected.²⁷ The external mass transfer in a well-mixed batch reactor was estimated based on the correlation reported by Sert et al.,³⁵ using Equation 13:

$$k_C = \frac{D_{\text{AC, M}}}{R_p} + 0.31 \times \left[\frac{\mu_M}{\rho_C \times D_{\text{AC, M}}} \right]^{-\frac{2}{3}} \times \left[\frac{(\rho_C - \rho_L) \times \mu_M \times g}{\rho_C^2} \right]^{\frac{1}{3}} \quad (13)$$

where $D_{\text{AC, M}}$ is the diffusivity of acetic acid in the liquid reaction mixture, μ_M is the viscosity of the reaction mixture, ρ_C is the density of the solid catalyst, and ρ_L is the density of liquid reaction mixture. The diffusivity was estimated using the multi-component diffusivity correlation according to the Perkin and Geankoplis method (Equation 14):³⁶

$$D_{\text{AC, M}} \times \mu_M^{0.8} = \sum_{j=1}^n x_j \times D_{\text{AC, j}} \times \mu_j^{0.8} \quad (14)$$

where $D_{\text{AC, j}}$ is the diluted binary diffusion coefficient of acetic acid in the component j (n-pentanol, pentyl ethanoate, and water, estimated using the Wilke–Chang correlation), x_j is the molar fraction of species j , and μ_j is the viscosity of species j . The values of μ_M and μ_j were obtained using the *Aspen Plus* v8.4 software (Aspen Technology, Inc.).

The influence of the internal mass transfer was determined based on the Weisz–Prater criterion (C_{WP}), defined by Equation 16,²⁷ where D_{EF} is effective diffusion of the acetic acid in the liquid phase mixture (Equation 15, where ξ is the porous tortuosity of the solid catalyst). For reaction systems with C_{WP} lower than 1.0, the internal mass transfer resistance can be neglected.

$$D_{EF} = \xi^2 \times D_{AC,M} \quad (15)$$

$$C_{WP} = \frac{r_{AC,OBS} \times \rho_C \times R_P^2}{D_{EF} \times C_{AC}} \quad (16)$$

3 | RESULTS AND DISCUSSION

3.1 | Catalyst characterization

Figure 1 summarizes the main characterization results for the synthesized catalyst. Figure 1A depicts the diffraction patterns for the sulfated zirconia, where the XRD spectrum shows the crystalline nature of the zirconia and the tetragonal phase (T) is predominant, as revealed by characteristic peaks highlighted in Figure 1A, at 30°, 35°, 50°, and 60°.^{37–39} Similarly, the predominance of the tetragonal phase was confirmed by the Raman shift (Figure 1B). According to Zyuzin et al⁴⁰ and Rabee et al,⁴¹ T-labeled peaks at 148, 267, 318, 462, 603, and 648 cm^{-1} , are due to various Zr–O lattice vibrations of ZrO_2 with the tetragonal phase. The predominance of this phase may have been favored by the zirconia precipitation procedure carried out with a high and constant pH (10). This result is expected according to Corma et al.³⁰ Moreover, the tetragonal phase of sulfated zirconia is desirable, because it leads to greater catalyst acidity and consequently a higher catalytic activity in acid esterification reactions.^{30,42}

FTIR spectrum for sulfated zirconia is shown in Figure 1C. A broad band can be observed at 3 000–3 600 cm^{-1} , assigned to the sample hydration, corresponding to the OH stretching vibration. The band at 1 625 cm^{-1} corresponds to δ HOH deformation, due to the presence of water coordinated to the material.^{39,43} Furthermore, a low-wavelength band (500–750 cm^{-1}) is assigned to Zr–O bonds.³⁹ Bands at 998, 1 044, 1 135, and 1 233 cm^{-1} indicate the presence of SO_4 . These bands are assigned to chelating bidentate sulfate ions coordinated to zirconium cations,⁴² which is probably responsible for the high acidity of Zr^{4+} , due to the sulfur–oxygen inductive effect.⁴⁴ The sulfate chelates a single Zr atom via a double oxygen bond, attracting electrons away and making it a strong Lewis acid.⁴⁵ Moreover, Brønsted acid sites can be formed and these contribute to the acid characteristic of this material. This occurs via sulfur bridges across two zirconium atoms and through water sorption the Lewis acid sites are converted to Brønsted acid sites.⁴⁶

Figure 1D presents the TGA and DSC curves for the sulfated zirconia, which show the high thermal stability of this material. The first weight loss (<4%) is characterized by an endothermic process on the DSC curve and is due to water loss through physisorption and chemisorption. Physisorbed water is released from room temperature to 120°C, while chemisorbed water is released between 300 and 500°C. The second weight loss begins at close to 600°C up to 850°C. This is an exothermic event and represents the decomposition of the sulfated metal oxide to give zirconium oxide and the volatile by-products sulfur dioxide and oxygen.⁴⁷

Particle size distribution of the synthesized sulfated zirconia (Figure 1E) indicates a material of small granulometry, ranging from 0.4 to 145 μm and the average particle diameter of 22.56 μm . The irregular size and shape of the catalyst particles can be observed in the SEM images (Figure 1F).

The elemental composition of the catalyst, obtained by EDS, was 52.86% \pm 3.00 Zr, 45.04% \pm 2.08 O, and 2.10% \pm 0.76 S, resulting in a value of 0.61 \pm 0.05 in term of SO_4 to ZrO_2 molar ratio. The chemical composition and properties of the sulfated zirconia depend on the ZrO_2 synthesis conditions and method for sulfation and calcination. However, similar results for the elemental composition of sulfated zirconia can be found in the work presented by Patel et al¹⁸ (58.96% Zr, 39.62% O, and 1.42% S). Moreover, Saravanan et al⁴⁸ obtained sulfated zirconia with 2.1 wt% of sulfur. The values for the BET surface area, pore volume and average pore diameter of the sulfated zirconia particles were 88.77 $\text{m}^2 \text{g}^{-1}$, 0.13 $\text{cm}^3 \text{g}^{-1}$, and 2.89 nm, respectively.

3.2 | Mass transfer phenomena

As mentioned above, a set of experiments with different stirring speed (50, 200, 500, and 700 rpm) were performed to evaluate the effect of the external mass transfer, and the results are presented in Figure 2. After 8 h, the acetic acid conversion was around 66% for the reactions performed with a stirring speed above 200 rpm. For the reaction carried out at 50 rpm, the conversion reached 58%. Lower reaction rate observed for the reaction at 50 rpm can be attributed to the low stirring speed the solid catalyst that was probably not well distributed inside the reactor.

Table 2 reports the Mears and Weisz–Prater criteria used to assesses the external and internal diffusion steps in the acetic acid esterification reaction catalyzed by sulfated zirconia, at temperatures of 50–80°C, and a stirring speed of 500 rpm. The Mears criterion values obtained varied within 1.32×10^{-4} and 2.45×10^{-4} . These values are significantly lower than 0.15 ($C_M \ll 0.15$), indicating that external diffusion is not the limiting step for the acetic acid reaction with n-pentanol over sulfated zirconia. Similarly, the Weisz–Prater values are significantly lower than one ($C_{WP} \ll 1$), which suggests that internal diffusion also does not limit the reaction. Both mass

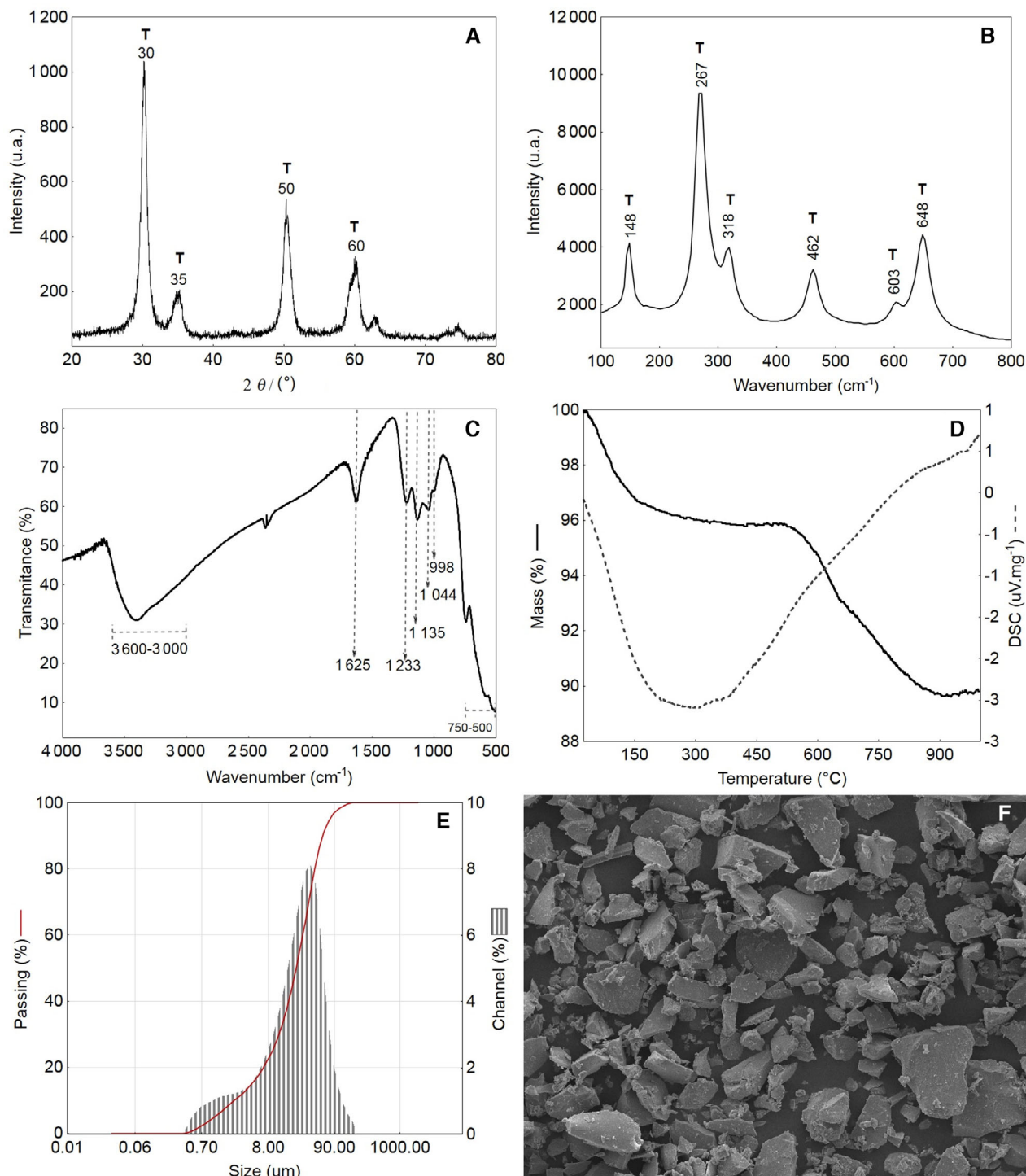


FIGURE 1 Catalyst characterization: (A) XRD patterns: T, tetragonal phase, (B) Raman spectra: T, tetragonal phase, (C) FTIR spectra, (D) thermogravimetric analysis, (E) particle size distribution, (F) SEM image with magnification 500 \times [Color figure can be viewed at wileyonlinelibrary.com]

transfer resistances can be neglected, mainly due to the small particle size of the catalyst, with an average diameter of 22.56 μm . Srilatha et al.²⁸ studied the esterification of palmitic acid with methanol catalyzed by a 12-tungstophosphoric acid support on ZrO_2 oxide and observed that external mass

transfer resistance was not relevant at stirring speeds above 400 rpm for a catalyst with an average particle size of 90 μm , while the internal mass transfer did not significantly affect the reaction rate for the catalyst particle size ranged of 0.4–145 μm .

TABLE 2 Significance of internal and external diffusion for different kinetics^a

Temperature (°C)	C_{AC} at 60 min (mmol cm ⁻³)	$r_{A,OBS}$ at 60 min (mol g ⁻¹ s ⁻¹)	D_{EF} (cm ² s ⁻¹)	k_C (cm s ⁻¹)	C_M	C_{WP}
50	2.35	4.12×10^{-6}	3.35×10^{-5}	2.97×10^{-2}	2.45×10^{-4}	1.23×10^{-4}
60	2.28	3.99×10^{-6}	4.02×10^{-5}	3.57×10^{-2}	2.04×10^{-4}	1.02×10^{-4}
70	2.04	3.57×10^{-6}	5.00×10^{-5}	4.43×10^{-2}	1.64×10^{-4}	8.22×10^{-5}
80	1.72	3.02×10^{-6}	6.24×10^{-5}	5.54×10^{-2}	1.32×10^{-4}	6.58×10^{-5}

^aCatalyst loading of 10 wt%, n-pentanol to acetic acid molar ratio of 3:1, stirring speed of 500 rpm.

C_{AC} , acetic acid concentration at 60 min in the kinetics.

$r_{A,OBS}$, experimental value of the reaction rate (mol g⁻¹ s⁻¹) at 60 min of reaction.

D_{EF} , effective coefficient diffusion; k_C , external mass transfer parameter; C_M , Mears criterion; C_{WP} , Weisz–Prater criterion.

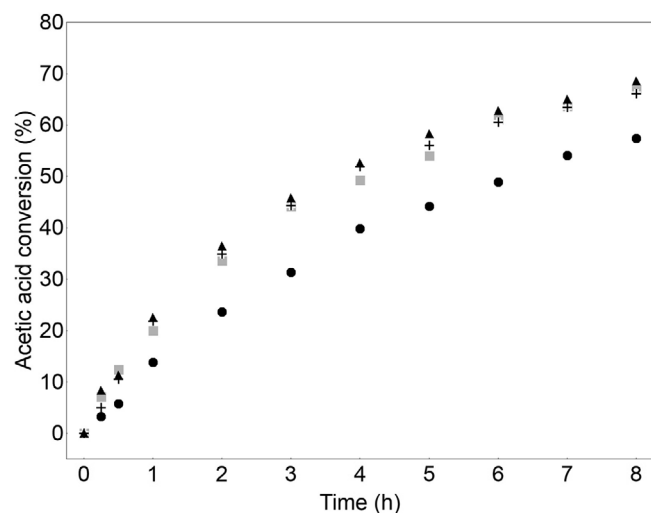


FIGURE 2 Effect of stirring speed (rpm) on acetic acid conversion at 70°C, catalyst loading of 10 wt%, n-pentanol to acetic acid molar ratio of 3:1. ●, 50 rpm; ■, 200 rpm; +, 500 rpm; ▲, 700 rpm

Therefore, as the external and internal mass transfer are not limiting step for the reaction evaluated in this work, the kinetic modeling can be performed considering the reaction as the limiting step for this heterogeneous catalysis, including the adsorption and desorption of the reactants in the catalyst surface.

3.3 | Effect of the variables on acetic acid conversion

Figure 3 shows the results obtained for the effects of the variables temperature and the n-pentanol to acetic acid molar ratio (MR) on the acetic acid conversion catalyzed by sulfated zirconia. In general, it can be observed that the reaction at a higher temperature and molar ratio favored the acetic acid conversion (Figure 3A). The Pareto chart in Figure 3B shows the estimated values for the effects based on the surface response regression, expressed on the right side of the bars. Factors that exceed the dashed line have a significant effect in terms of acetic acid conversion ($P < .05$). The assessment

of the effects indicated that the temperature is the most significant factor in the acetic acid conversion through the esterification reaction with n-pentanol, with a P value of .0267. The molar ratio was not significant with a confidence level of $P = .05$, within the range evaluated. Even though the ANOVA suggested that the results obtained varying the molar ratio were not statistically different, it can be observed in Figure 3A that the maximum reaction conversion was obtained at a molar ratio of 3:1 and temperature of 80°C, suggesting that an excess of the alcohol favors the pentyl ethanoate synthesis. However, as confirmed by the statistical analysis, a high amount of alcohol excess is not necessary to promote a shift in the reaction and increase the acetic acid conversion, while an increase in the temperature favored the reaction rate allowing higher conversions obtained for the same reaction time and catalyst amount.

Figure 4A depicts the kinetics of the acetic acid esterification with sulfated zirconia (10 wt%) at 70°C and different n-pentanol to acetic acid molar ratios. As discussed above, an excess of alcohol did not improve the acetic acid conversion for a long period of reaction. The acetic acid conversions obtained after 8 h at n-pentanol to acetic acid molar ratios of 2:1 and 3:1 were 65.9% and 66.1%, respectively.

The effect of the catalyst concentration was also evaluated at 70°C, with a fixed n-pentanol to acetic acid molar ratio of 3:1. In Figure 4B can be observed that a higher amount of catalyst, in the range evaluated, led to higher acetic acid conversions. It can be observed that the conversion of acetic acid increased almost proportionally with the catalyst loading after 2 h. As expected, a higher catalyst loading leads to an increase in the amount of available active sites for the reaction, affecting the adsorption and surface reaction step in the catalyst mechanism.

Figure 5 depicts a comparison for the kinetics of acetic acid and n-pentanol esterification using homogeneous and heterogeneous catalyst. The effect of temperature on the acetic acid esterification can be observed in Figure 5A for the homogeneous catalysis with H₂SO₄ (1 wt%), while the reaction catalyzed by sulfated zirconia (10 wt%) is presented in Figure 5B. The homogeneous reaction resulted in a faster conversion compared with the use of a heterogeneous catalyst

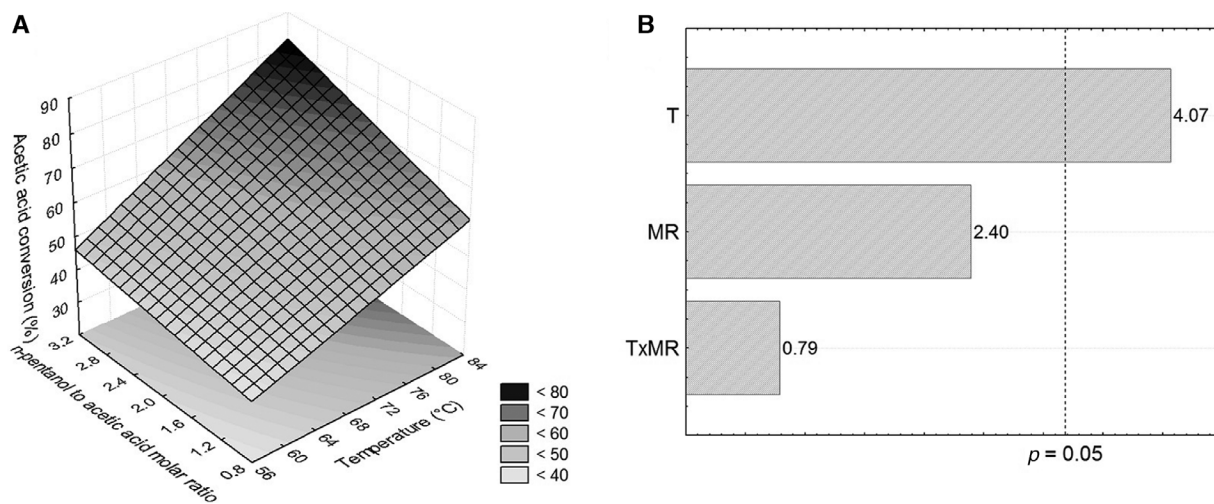


FIGURE 3 (A) Response surface plot showing the effect of temperature and molar ratio, on the acetic acid conversion. (B) Estimative of variables in acetic acid conversion. The percentage of catalyst is constant (10 wt%). The reactions were conducted by 6 h

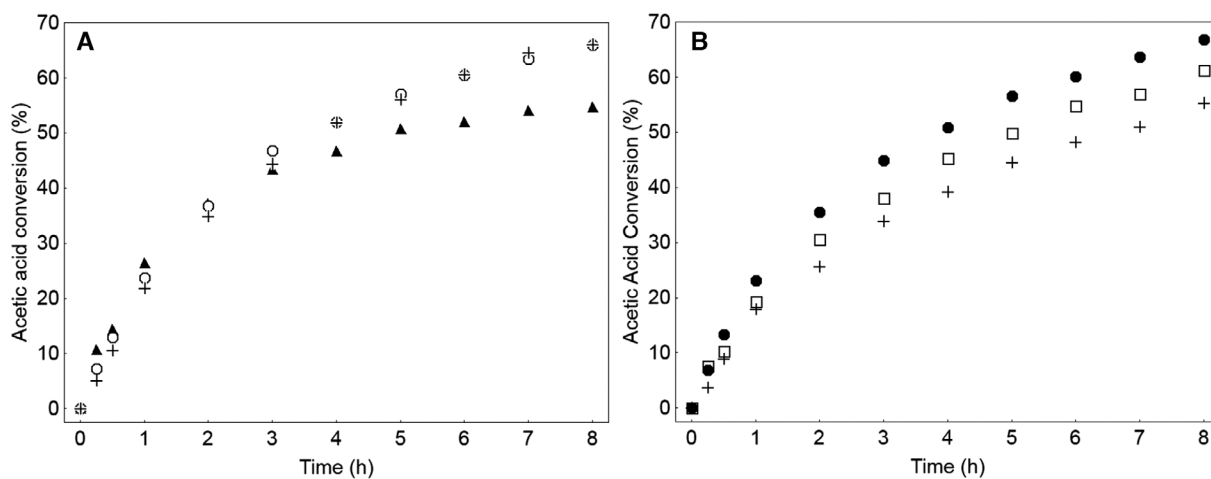


FIGURE 4 (A) Kinetic of acetic acid esterification with n-pentanol by sulfated zirconia over different n-pentanol to acetic acid molar ratio: \blacktriangle , 1:1; $+$, 2:1; \circ , 3:1 ($T = 70^\circ\text{C}$, catalyst loading of 10 wt%), (B) different catalyst loading: $+$, 5 wt%; \square , 7.5 wt%; \bullet , 10 wt% ($T = 70^\circ\text{C}$, molar ratio of n-pentanol/acetic acid 3:1)

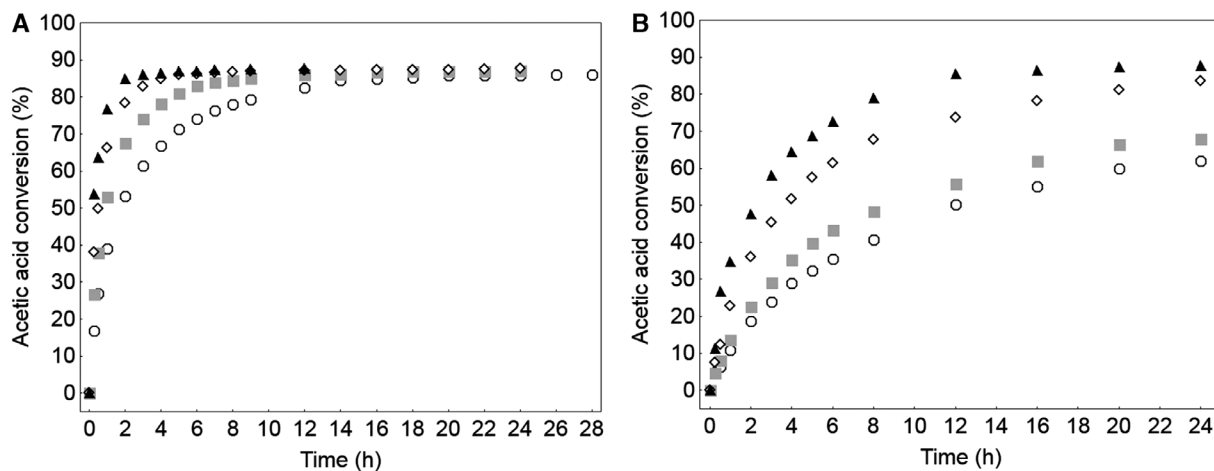


FIGURE 5 Kinetic of acetic acid esterification with n-pentanol by sulfated zirconia over different temperatures: \circ , 50°C; \blacksquare , 60°C; \diamond , 70°C; \blacktriangle , 80°C. (A) Homogeneous catalysis (H_2SO_4 at 1 wt%), (B) heterogeneous catalysis with sulfated zirconia (10 wt%)

TABLE 3 Equilibrium conversion and enthalpy of reaction^a

Temperature (°C)	Equilibrium conversion (X_{EQ}) ^b	Equilibrium constant (K_{EQ})	ΔH° (kJ mol ⁻¹)
50	0.902	28.63	
60	0.897	26.48	-8.49
70	0.891	24.46	
80	0.885	21.65	

^aH₂SO₄ catalyst loading of 1 wt%, n-pentanol to acetic acid molar ratio of 3:1, stirring speed of 500 rpm.

^bEquilibrium conversion data obtained by simulation with software Aspen Plus v8.4.

for the operational conditions evaluated. This is expected, as the nucleophilic attack of the alcohol on the protonated carbonyl group of the carboxylic acid occurs in the whole reaction mixture, due to the homogeneous phase between the reactant and strong mineral acid (H₂SO₄). In the heterogeneous catalyst, this step occurs only at the active Lewis and Brønsted acid sites of the solid catalyst, and is thus dependent on the amount of solid catalyst added to the system along with its morphology (structural, textural and acidic properties).⁹ In this study, the maximum acetic acid conversion obtained at 50 and 80°C was 86.7% and 88.3%, respectively, while the equilibrium conversion estimated by software *Aspen Plus* v8.4 was 90.2% and 88.5% (Table 3), at the same temperatures. These results suggest that an increase in the temperature increases the rate of collisions between the reactants (in the homogeneous reaction) or between the reactants and the active sites of the catalyst (in the heterogeneous reaction), promoting a faster reaction, that is, reducing the residence time required to approximate equilibrium conversions, even that the equilibrium conversion showed a slight decrease with temperature (from 90.2% at 50°C to 88.5% at 80°C).

Table 3 reports the values for the equilibrium conversion of acetic acid and the equilibrium constant for the esterification reaction. Both showed a small decrease within the temperature range evaluated, suggesting an exothermic reaction and that the equilibrium reaction is not strongly dependent on temperature. The estimated enthalpy of reaction was -8.49 kJ mol⁻¹, also suggesting a slightly exothermic reaction in the temperature range evaluated. Similar result was reported by Sert and Ataly¹¹ for acetic acid esterification with n-butanol (-18.7 kJ mol⁻¹) and Ali et al² for the esterification of propionic acid with n-propanol (-6.4 kJ mol⁻¹), although other studies have reported endothermic behavior, as presented Liu and Tan⁴⁹ for propionic acid esterification with n-butanol (+1.92 kJ mol⁻¹), and Jyoti et al⁵⁰ for acrylic acid esterification with ethanol (+2.35 kJ mol⁻¹). Such differences reported in the literature can be attributed at the approaches used to estimate the equilibrium conversions concerning the pure component parameters and thermodynamic models used in these calculations. However, all cited studies reported low

values for enthalpy of the reaction, which is suggesting a weakly temperature-dependent reaction in liquid phase.¹¹

3.4 | Kinetics modeling of sulfated zirconia-catalyzed esterification

The heterogeneous, PH, LH, and ER kinetic models with different controlling steps (Table 1) were applied to correlate the kinetics data obtained for the temperature range of 50-80°C. The values of mean relative errors (MRE) and root mean square deviation (RMSD) obtained for the different kinetic models used are reported in Table 4. The PH model did not show satisfactory agreement with the experimental data, suggesting that the reaction mechanism is dependent on the interaction between the reactants and the active acid sites of the sulfated zirconia. The surface reaction models based on the LH (LH_RS) and ER (ER_AC_RS and ER_P_RS) theories showed good fits to the kinetics data, with the lowest values for the mean relative errors (1.1% and 3.1%, respectively) and the root mean square deviation (0.4% and 1.9%, respectively). These results suggest that the step of the surface reaction at the active acid sites is the limiting step of the reaction mechanism.

In order to evaluate the most adequate reaction mechanism to describe the acetic acid esterification with n-pentanol over sulfated zirconium oxide, the Fisher's *F*-test (*F*) and AIC were adopted. Table 5 reports the *F* and AIC values for the surface reaction models based on LH (LH_RS) and ER (ER_AC_RS and ER_P_RS) theories.

As reported in Tables 4 and 5, the models of LH and ER with acetic acid adsorbed showed a good fit in correlating the experimental kinetic data of acetic acid and n-pentanol esterification over sulfated zirconia. Osatiashtiani et al⁵¹ suggest the mechanism of esterification reaction between carboxyl acids and light aliphatic alcohols catalyzed by sulfated zirconia occurs between 02 vicinal Brønsted sites, among the nucleophilic species generated from the coordinations of alcohol and acid onto the Brønsted active sites of ZrO₂. Other studies, however, suggest the presence of Lewis acid sites induces the interaction of one of the reactants with the active site and the nucleophilic attack by the other free reactant.^{11,19,48} Sert and Ataly¹¹ identify the Eley-Rideal (with acetic acid adsorbed onto the active acid sites) theory as the model more suitable to describe the esterification of acetic acid with n-butanol catalyzed by sulfated zirconia. Sankar et al¹⁹ suggested ER (with levulinic acid adsorbed) as plausible reaction mechanism for esterification of levulinic acid over ZrO₂/SBA-15. Saravanan et al⁴⁸ suggested the ER theory to describe the mechanism of the kinetic of esterification of stearic acid with methanol over sulfated zirconia, where the Lewis acid route consists of the direct coordination of the carboxyl group of a carboxyl acid to the Zr⁺ acid site, followed by a nucleophilic attacked by the oxygen of the alcohol and the

TABLE 4 Mean relative errors (MRE) and root mean square deviation (RMSD) for different reaction mechanisms at different reaction temperatures^a

Model	50°C		60°C		70°C		80°C	
	MRE (%)	RMSD (%)	MRE (%)	MRE (%)	MRE (%)	RMSD (%)	MRE (%)	RMSD (%)
PH	12.4	7.2	12.1	5.6	15.1	6.6	8.4	5.6
LH_AD_AC	8.0	2.3	4.9	5.3	3.5	1.6	4.0	2.5
LH_AD_P	12.5	2.3	1.7	1.0	6.0	4.8	9.4	7.2
LH_SR	2.0	0.5	1.4	0.8	1.1	0.5	3.1	2.2
LH_DES_E	15.7	4.0	2.9	1.2	6.0	3.3	5.1	3.2
LH_DES_W	21.8	8.5	15.4	10.9	13.8	9.3	12.4	8.7
ER_AC_ADS	4.5	1.4	1.8	0.9	3.0	1.4	2.8	1.8
ER_AC_RS	2.6	0.8	1.1	0.7	1.8	0.8	2.4	1.7
ER_AC_DES_E	8.1	4.3	9.1	5.5	9.9	5.9	4.5	3.0
ER_AC_DES_W	14.7	5.2	11.1	5.8	6.8	4.3	3.3	2.1
ER_P_ADS	5.7	1.6	2.8	2.4	6.0	5.8	8.6	6.3
ER_P_RS	3.2	0.9	1.1	0.7	2.6	1.0	3.3	2.1
ER_P_DES_E	13.9	5.4	8.8	5.6	6.8	3.8	2.8	1.8
ER_P_DES_W	15.3	5.5	5.0	3.0	10.7	5.1	2.7	1.8

^an-pentanol to acetic acid molar ratio of 3:1 and catalyst loading of 10 wt%.

TABLE 5 Fischer *F*-test (*F*) and Akaike criteria (AIC) for chosen the model between surface reaction models based on Langmuir–Hinshelwood and Eley–Rideal theories^a

Model	50°C		60°C		70°C		80°C	
	<i>F</i>	AIC	<i>F</i>	AIC	<i>F</i>	AIC	<i>F</i>	AIC
LH_SR	3 262	−118	1 985	−106	21 152	−138	1 964	−98
ER_AC_RS	1 627	−116	3 785	−121	17 064	−125	6 202	−113
ER_P_RS	1 502	−114	3 164	−120	12 460	−121	4 189	−107

^aKinetic data obtained at different temperatures, n-pentanol to acetic acid molar ratio of 3:1 and catalyst loading of 10 wt%.

deprotonation and water loss releasing the ester formed; while the Brønsted acid catalyzed mechanism consists of the transfer of H⁺ from the ZrO₂ acid site to the carbonyl group of the carboxyl acid, followed by a nucleophilic attack of the oxygen from the alcohol, deprotonation and water loss followed by the formation of the ester product.

Both models consider the hypotheses that all active acid sites are uniform and with equal energy, and the one of the adsorbed acid site does not influence the activity of the vicinal acid site,²⁷ but both models did not evaluate the presence and activity of different kind of active acid sites or the heterogeneous morphology reported at Figure 1. Due to the non-ideality of the catalyst and reaction system, hypotheses assumed by the models employed in this study, and the results observed from the fitted models on the experimental data, it is reasonable consider that esterification under sulfated zirconia could occur by both LH and by ER concept.

According with the Akaike's criteria, the ER_AC_RS showed more significant mathematical model to represent the esterification reaction herein studied, once it requires less parameters, provided the lowest AIC values and the highest *F*

TABLE 6 Kinetic constant and adsorption parameters for ER_AC_RS mechanism

Temperature (°C)	$k_f \times 10^2$ (mol g ^{−1} min ^{−1})	K_{AC}	K_W
50	0.856	0.379	14.690
60	1.4330	0.370	13.239
70	2.668	0.356	12.890
80	4.813	0.321	12.530

values for set of experimental data obtained at 60 and 80°C. Moreover, for set of experimental data obtained at 50 and 70°C, the ER_AC_RS showed as good as the LH model.

Figure 6 presents a comparison between the experimental data and predicted values obtained from the ER_AC_RS model with the surface reaction as the limiting step, for the temperatures from 50 to 80°C. The predicted values for the acetic acid conversion are in good agreement with the experimental data in the temperature range evaluated in this study. The kinetics parameters and adsorption equilibrium constants are reported in Table 6.

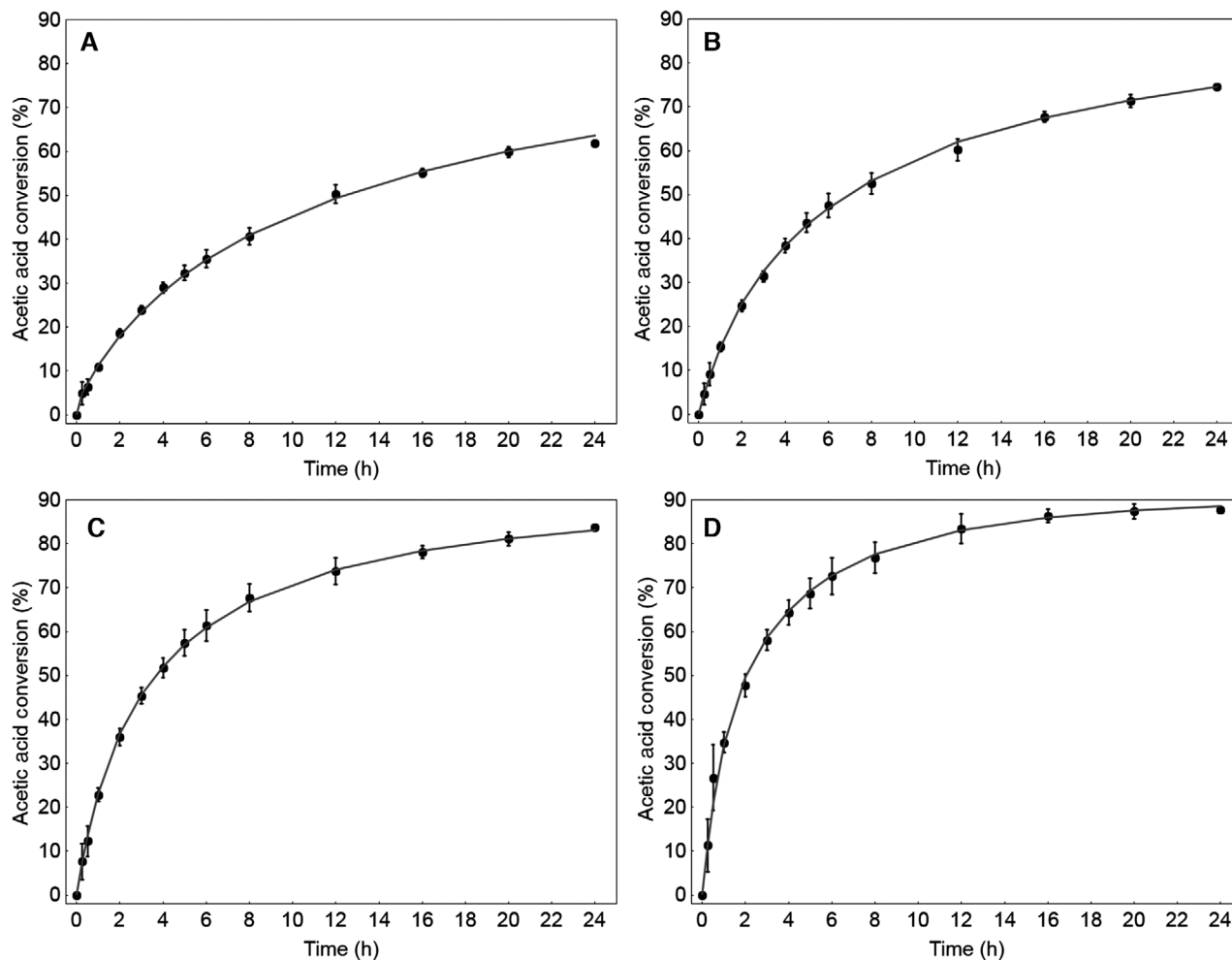


FIGURE 6 Kinetics of acetic acid esterification with n-pentanol by sulfated zirconia over different temperature: (A) 50°C, (B) 60°C, (C) 70°C, and (D) 80°C. Line is the kinetic model and ● is the experimental data

Based on the fitting of the Arrhenius-like expression (Eq. 6), the activation energy was found to be 55.6 kJ mol⁻¹, which is of the same order of magnitude of activation energy observed in other reaction systems catalyzed by sulfated zirconia: Yadav and Kundu¹⁴ (85.7 kJ mol⁻¹) for alkylation of diphenyl oxide with 1-decene, Omota et al¹⁷ (66.5 kJ mol⁻¹) for esterification of dodecanoic acid with 2-ethylhexanol, Sert and Ataly¹¹ (49 kJ mol⁻¹) for the esterification of acetic acid with n-butanol, both catalyzed by sulfated zirconia. As comparison, the results obtained in our study are in the same order of other catalyst usually employed in esterification reactions: Ali et al² (67.3 kJ mol⁻¹) for esterification of propionic acid with n-propanol catalyzed with ion-exchange resin Dowex 50Wx8-400, Santos et al²⁵ (123.1 kJ mol⁻¹) for esterification of lauric acid ethanol catalyzed by acid activated montmorillonite (STx1-b).

Kinetic parameters and adsorption equilibrium constant reported in Table 6 indicate that the affinity of water for the active acid sites is higher than for the acetic acid, and this decreases as the reaction temperature increases. The infer-

ence is that esterification occurs by the nucleophilic attack of the n-pentanol on acetic acid adsorbed onto the Lewis acid sites (Zr⁺) and Brønsted acid sites (H⁺), and that the presence of water decreases the reaction rates by competitive adsorption on the acid sites. A high reaction temperature reduces the adsorption interaction between water and the active acid sites and increases the surface reaction rates, promoting higher conversions.

4 | CONCLUSIONS

The kinetics data obtained regarding the esterification of acetic acid with n-pentanol, using sulfated zirconia as a catalyst, to obtain pentyl ethanoate indicated that an increase in temperature and catalyst loading were favorable to the ester formation. Moreover, higher temperature led to a slight decrease in the acetic acid equilibrium conversion and in the reaction equilibrium constant. The estimated enthalpy of the

reaction was $-8.49 \text{ kJ mol}^{-1}$, suggesting a slightly exothermic reaction. The models of LH and ER with acetic acid adsorbed onto the active sites, considering the reaction surface as the limiting step, showed good fit of the experimental data, but by the Akayke's criteria, the ER model showed to be most capable model to describe the kinetics of the reaction mechanism involved in the esterification of acetic acid with n-pentanol over sulfated zirconia.

ORCID

Vitor Renan da Silva 

<https://orcid.org/0000-0002-0109-4155>

Marcos Lúcio Corazza 

<https://orcid.org/0000-0003-2305-1989>

REFERENCES

1. Yadav GD, Mehta PH. Heterogeneous catalysis in esterification reactions: preparation of phenethyl acetate and cyclohexyl acetate by using a variety of solid acidic catalysts. *Ind Eng Chem Res.* 1994;33:2198-2208.
2. Ali SH, Sabiha QM, Al-Sahhaf T. Synthesis of esters: Development of the rate expression for the Dowex 50 Wx8-400 catalyzed esterification of propionic acid with 1-propanol. *Chem Eng Sci.* 2007; 62:3197-3217.
3. Marx S. Glycerol-free biodiesel production through transesterification: a review. *Fuel Process Technol.* 2017;151: 139-147.
4. Murad PC, Hamerski F, Corazza ML, Luz LFL, Voll FAP. Acid-catalyzed esterification of free fatty acids with ethanol: an assessment of acid oil pretreatment, kinetic modeling and simulation. *React Kinet Mech Catal.* 2018;123:505-515.
5. Hamerski F, Corazza ML. LDH-catalyzed esterification of lauric acid with glycerol in solvent-free system. *Appl Catal A Gen.* 2014;475:242-248.
6. Hu K, Jin GJ, Mei WC, Li T, Tao YS. Increase of medium-chain fatty acid ethyl ester content in mixed *H. uvarum*/S. cerevisiae fermentation leads to wine fruity aroma enhancement. *Food Chem.* 2018;239:495-501.
7. Gunathilake M, Shimmura K, Dozen M, Miyawaki O. Flavor retention in progressive freeze-concentration of coffee extract and pear (La France) juice flavor condensate. *Food Sci Technol Res.* 2014;20:547-554.
8. Rossi SC, Medeiros ABP, Weschenfelder TA, Scheer AP, Soccol CR. Use of pervaporation process for the recovery of aroma compounds produced by P. fermentans in sugarcane molasses. *Bioprocess Biosyst Eng.* 2017;40:959-967.
9. Umrigar V, Chakraborty M, Parikh P. Esterification and ketalization of levulinic acid with desilicated zeolite β and pseudo-homogeneous model for reaction kinetics. *Int J Chem Kinet.* 2019;51:299-308.
10. Khudsange CR, Wasewar KL. Kinetics, mass transfer, and thermodynamic and statistical modeling study for esterification of valeric acid with n-butanol: Homogeneous and heterogeneous catalysis. *Int J Chem Kinet.* 2018;50:710-725.
11. Sert E, Ataly FS. Kinetic study of the esterification of acetic acid with butanol catalyzed by sulfated zirconia. *React Kinet Mech Catal.* 2010;99:125-134.
12. Wang X, Wang H, Liu Y, Liu F, Yu Y, He H. A direct sulfation method for introducing the transition metal cation Co^{2+} into ZrO_2 with little change in the Brønsted acid sites. *J Catal.* 2011;279:301-309.
13. Arata K. Organic syntheses catalyzed by superacidic metal oxides: sulfated zirconia and related compounds. *Green Chem.* 2009;11:1719-1728.
14. Yadav GD, Kundu B. Friedel-Crafts alkylation of diphenyl oxide with 1-decene over sulfated zirconia as catalyst. *Can J Chem Eng.* 2001;79:805-811.
15. Osatiashtiani A, Lee AF, Brown DR, Melero JA, Morales G, Wilson K. Bifunctional SO_4/ZrO_2 catalysts for 5-hydroxymethylfurfural (5-HMF) production from glucose. *Catal Sci Technol.* 2014;4:333-342.
16. Popova SA, Chukicheva IY, Kutchin AV, Tarasov AL, Kustov LM. Sulfated zirconia-catalyzed alkylation of phenol with camphene and isomerization of n-butane. *Mendeleev Commun.* 2014;24:98-99.
17. Omota F, Dimian AC, Blick A. Fatty acid esterification by reactive distillation: Part 2 – kinetics-based design for sulphated zirconia catalysts. *Chem Eng Sci.* 2003;58:3175-3185.
18. Patel A, Brahmkhatri V, Singh N. Biodiesel production by esterification of free fatty acid over sulfated zirconia. *Renew Energy.* 2013;51:227-233.
19. Sankar ES, Mohan V, Suresh M, Saidulu G, Raju BD, Rama RKS. Vapor phase esterification of levulinic acid over $\text{ZrO}_2/\text{SBA-15}$ catalyst. *Catal Commun.* 2016;75:1-5.
20. Unlu D, Ilgen O, Hilmioglu ND. Biodiesel additive ethyl levulinate synthesis by catalytic membrane: $\text{SO}_4^{-2}/\text{ZrO}_2$ loaded hydroxyethyl cellulose. *Chem Eng J* 2016;302:260-268.
21. Alegria A, Cuellar J. Esterification of oleic acid for biodiesel production catalyzed by 4-dodecylbenzenesulfonic acid. *Appl Catal B Environ.* 2015;179:530-541.
22. Hamerski F, Prado MA, Silva VR, Voll FAP, Corazza ML. Kinetics of layered double hydroxide catalyzed esterification of fatty acids with glycerol. *React Kinet Mech Catal.* 2016;117:253-268.
23. Lee MJ, Wu HT, Lin HM. Kinetics of catalytic esterification of acetic acid and amyl alcohol over Dowex. *Ind Eng Chem Res.* 2000;39:4094-4099.
24. Ju IB, Lim HW, Jeon W, Suh DJ, Park MJ, Suh YW. Kinetic study of catalytic esterification of butyric acid and n-butanol over Dowex 50Wx8-400. *Chem Eng J.* 2011;168:293-302.
25. Santos PRS, Wypych F, Voll FAP, Hamerski F, Corazza ML. Kinetics of ethylic esterification of lauric acid on acid activated montmorillonite (STx1-b) as catalyst. *Fuel.* 2016;181:600-609.
26. Chandane VS, Rathod AP, Wasewar KL, Sonawane SS. Esterification of propionic acid with isopropyl alcohol over ion exchange resins: optimization and kinetics. *Korean J Chem Eng.* 2017;34:249-258.
27. Fogler SH. *Elements of Chemical Reaction Engineering.* New-York: Prentice-Hall; 1999. 967 p.
28. Srilatha K, Lingaiah N, Sai Prasad PS, Prabhavathi Devi BLA, Prasad RBN Kinetics of the esterification of palmitic acid with methanol catalyzed by 12-tungstophosphoric acid supported on ZrO_2 . *React Kinet Mech Catal.* 2011;104:211-226.
29. Yan GX, Wang A, Wachs IE, Baltrusaitis J. Critical review on the active site structure of sulfated zirconia catalyst and prospects in fuel production. *Appl Catal A.* 2019;572:210-225.
30. Corma A, Fornés V, Juan-Rajadell MI, López Nieto JM. Influence of preparation conditions on the structure and catalytic properties of $\text{SO}_4^{-2}/\text{ZrO}_2$ superacid catalysts. *Appl Catal A.* 1994;116:151-163.

31. Brunauer S, Emmett PH, Teller E. Adsorption of gases in multi-molecular layers. *J Am Chem Soc.* 1938;60:309-319.
32. Riechert O, Husham M, Sadowski G. Solvent effects on esterification equilibria. *AIChE J.* 2015;61:3000-3011.
33. Molinero L, Ladero M, Tamayo JJ, Garcia-Ochoa F. Homogeneous catalytic esterification of glycerol with cinnamic and methoxycinnamic acids to cinnamate glycerides in solvent less medium: kinetic modeling. *Chem Eng J.* 2014;247:174-182.
34. Lee LS, Liang SJ. Phase and reaction equilibria of acetic acid–1-pentanol–water–n-amyl acetate system at 760 mmHg. *Fluid Phase Equilib.* 1998;149:57-74.
35. Sert E, Bulukulu AD, Karakus S, Atalay FS. Kinetic study of catalytic esterification of acrylic acid with butanol catalyzed by different ion exchange resins. *Chem Eng Process.* 2013;73:23-28.
36. Perry RH, Green DW. *Perry's Chemical Engineers' Handbook.* New York: McGraw-Hill, 1997. 2641 p.
37. Kuwahara Y, Kaburagi W, Nemoto K, Fujitani T. Esterification of levulinic acid with ethanol over sulfated Si-doped ZrO₂ solid acid catalyst: Study of the structure–activity relationships. *Appl Catal A.* 2014;476:186-196.
38. Popova M, Szegedi A, Lazarova H, et al. Influence of the preparation method of sulfated zirconia nanoparticles for levulinic acid esterification. *React Kinet Mech Catal.* 2017;120:55-67.
39. Raia RZ, Silva LS, Marcucci SMP, Arroyo PA. Biodiesel production from *Jatropha curcas* L. oil by simultaneous esterification and transesterification using sulphated zirconia. *Catal Today.* 2017;289:105-114.
40. Zyuzin DA, Cherepanova SV, Moroz EM, et al. X-ray, Raman and FTIRS studies of the microstructural evolution of zirconia particles caused by the thermal treatment, *J Solid State Chem.* 2006;179:2965-2971.
41. Rabee AIM, Mekhemer GAH, Zaki MI. Spectro-thermal characterization of the nature of sulfate groups immobilized on tetragonal zirconium oxide: Consequences of doping the oxide with Al or Mg cations. *Thermochim Acta.* 2019;674:1-9.
42. Sun Y, Ma S, Du Y, et al. Xiao F. Solvent-free preparation of nano-sized sulfated zirconia with brønsted acidic sites from a simple calcination. *J Phys Chem.* 2005;109:2567-2572.
43. Ardizzone S, Bianchi CL, Cappelletti G, Porta F. Liquid-phase catalytic activity of sulfated zirconia from sol–gel precursors: the role of the surface features. *J Catal.* 2004;227:470-478.
44. Yadav GD, Nair JJ. Sulfated zirconia and its modified versions as promising catalysts for industrial processes. *Microporous Mesoporous Mater.* 1999;33:1-48.
45. Yamaguchi T. Recent progress in solid superacid. *Appl Catal.* 1990;61:1-25.
46. Clearfield A, Serrette GPD, Khazi-Syed AH. Nature of hydrous zirconia and sulfated hydrous zirconia. *Catal Today.* 1994;20:295-312.
47. Liu N, Guo X, Navrotsky A, Shi L, Wu D. Thermodynamic complexity of sulfated zirconia catalysts. *J Catal.* 2016;342:158-163.
48. Saravanan K, Tyagi B, Bajaj HC. Nano-crystalline, mesoporous aerogel sulfated zirconia as an efficient catalyst for esterification of stearic acid with methanol. *Appl Catal B Environ.* 2016;192:161-170.
49. Liu WT, Tan CS. Liquid-phase esterification of propionic acid with n-butanol. *Ind Eng Chem Res.* 2001;40:3281-3286.
50. Jyoti G, Keshav A, Anadkumar J. Experimental and kinetic study of esterification of acrylic acid with ethanol using homogeneous catalyst. *Int J Chem React Eng.* 2016;14:571-578.
51. Osatiashitiani LJA, Durnell JC, Manayil AFJ, Lee AF, Wilson K. Influence of alkyl chain length on sulfated zirconia catalyzed batch and continuous esterification of carboxylic acids with light alcohols. *Green Chem.* 2016;18:5529-5535.

SUPPORTING INFORMATION

Additional supporting information may be found online in the Supporting Information section at the end of the article.

How to cite this article: Hamerski F, Dusi GG, Fernandes dos Santos JT, da Silva VR, Voll FAP, Corazza ML. Esterification reaction kinetics of acetic acid and n-pentanol catalyzed by sulfated zirconia. *Int J Chem Kinet.* 2020;1-14. <https://doi.org/10.1002/kin.21365>